Applied Physics Letters

High-temperature tunneling electroresistance in metal/ferroelectric/ semiconductor tunnel junctions

Cite as: Appl. Phys. Lett. **111**, 132905 (2017); https://doi.org/10.1063/1.4999270
Submitted: 07 August 2017 . Accepted: 15 September 2017 . Published Online: 27 September 2017

Zhongnan Xi, Qiao Jin, Chunyan Zheng, Yongcheng Zhang, Chaojing Lu, Qiang Li, Shandong Li, Jiyan Dai, and Zheng Wen

High-temperature tunneling electroresistance in metal/ferroelectric/semiconductor tunnel junctions

Zhongnan Xi,[1] Qiao Jin,[1] Chunyan Zheng,[1] Yongcheng Zhang,[1] Chaojing Lu,[1] Qiang Li,[1] Shandong Li,[1] Jiyan Dai,[2] and Zheng Wen[1,2,a)]
[1]College of Physics, Qingdao University, Qingdao 266071, China
[2]Department of Applied Physics, The Hong Kong Polytechnic University, Hong Kong 999077, China

(Received 7 August 2017; accepted 15 September 2017; published online 27 September 2017)

Recently, ferroelectric tunnel junctions (FTJs) have attracted great attention due to promising applications in non-volatile memories. In this study, we report high-temperature tunneling electroresistance (TER) of metal/ferroelectric/semiconductor FTJs. Hysteretic resistance-voltage loops are observed in the Pt/$BaTiO_3$/Nb:$SrTiO_3$ tunnel junction from 300 to 513 K due to the modulation of interfacial Schottky barrier by polarization switching in the 4 u.c.-thick $BaTiO_3$ barrier via a ferroelectric field effect. The Pt/$BaTiO_3$/Nb:$SrTiO_3$ device exhibits a giant R_{OFF}/R_{ON} resistance ratio of $\sim 3 \times 10^5$ at 383 K and maintains bipolar resistance switching up to 513 K, suggesting excellent thermal endurance of the FTJs. The temperature-dependent TER behaviors are discussed in terms of the decrease of polarization in the $BaTiO_3$ barrier, and the associated junction barrier profiles are deduced by transport and capacitance analyses. In addition, by extrapolating the retention time at elevated temperature in an Arrhenius-type relation, activation energy of ~0.93 eV and room-temperature retention time of ~70 years can be extracted. *Published by AIP Publishing*. [http://dx.doi.org/10.1063/1.4999270]

Ferroelectric tunnel junctions (FTJs) have the advantages of non-destructive readout, high-density data storage, fast write/read access, and low power consumption.[1,2] In an FTJ, the overall potential profile seen by electrons can be altered by polarization switching in a ferroelectric barrier, which gives rise to a resistance switching of the device between a high (OFF) and a low (ON) level, i.e., the so-called tunneling electroresistance (TER), manifesting itself as a R_{OFF}/R_{ON} resistance ratio.[3,4] Recently, electroresistance mechanisms of the FTJs have been theoretically modeled[3–6] and giant TER performances have been experimentally realized in various device structures.[7–17] By employing $BiFeO_3$, which has a large spontaneous polarization, Bruno *et al.* have observed a room-temperature R_{OFF}/R_{ON} ratio of $\sim 10^5$ in Pt/Co/$BiFeO_3$/$LaNiO_3$ FTJs.[11] Besides, greatly enhanced TER has been achieved by exploring interfacial electric-field effects,[12–17] such as the metal-insulator phase transition in ultrathin $(La_{0.5}Ca_{0.5})MnO_3$ insertion in $(La_{0.7}Sr_{0.3})MnO_3$/$(La_{0.5}Ca_{0.5})MnO_3$/$BaTiO_3$ (BTO)/$(La_{0.7}Sr_{0.3})MnO_3$ tunnel junctions[12] and the Schottky barrier modulation in metal/ferroelectric/semiconductor (MFS) FTJs.[16,17] These results suggest great potential of the FTJs as alternative non-volatile memory designs for the mainstream FLASH devices that is expected to run into physical limits in the near feature.[18]

In integrated circuits, self-heating effect is unavoidable, and memory cells are always operating above room temperature. Thermal endurance is thus an important issue for practical devices, which has been investigated not only in FLASH devices[19–21] but also in ferroelectric random access memories (FeRAMs) based on thick ferroelectric films.[22–24] In FTJs, however, the memory performance may be more susceptible to temperature since the critical temperature for ferroelectric-paraelectric transition and the domain size are expected to decrease in ultrathin ferroelectric barriers.[25,26] Therefore, we study high-temperature TER of FTJ devices in the present work from 300 to 513 K. The MFS-type Pt/BTO/Nb:$SrTiO_3$ FTJs are adopted due to their giant TER at room temperature. A R_{OFF}/R_{ON} ratio as high as $\sim 3 \times 10^5$, close to that of Flash memories,[27,28] can be maintained up to 383 K, exceeding the typical operation temperature (~358 K) of integrated circuits.[19] Temperature-dependent TER behaviors of the Pt/BTO/Nb:$SrTiO_3$ are investigated considering electron transport with an evolving interfacial Schottky barrier and a decreasing polarization in the 4 u.c.-thick BTO barrier as temperature increases.

The BTO ultrathin films were epitaxially grown on *n*-type single-crystalline (001) Nb:$SrTiO_3$ (NbSTO, Nb: 0.7 wt. %) substrates by pulsed laser deposition, as reported previously.[29] Ferroelectric properties of the BTO/NbSTO heterostructure were measured by the means of piezoresponse force microscopy (PFM) using an Asylum Research Cypher scanning probe microscope with conductive Pt/Ti-coated tip as top electrode. Pt top electrodes of ~30 μm in diameter and ~50 nm in thickness were deposited on the surface of BTO/NbSTO by sputtering with a shadow mask to form the FTJ device. Resistance switching was measured by A Keithley 2400 SourceMeter, and capacitance was recorded using an Agilent 4294A impedance analyzer with a frequency of 3 MHz and an oscillation level of 30 mV. The testing pulses were applied to the Pt electrode, and the NbSTO substrate was always grounded through an indium ohmic contact pad.

The 4 u.c.-thick BTO film is grown coherently on the NbSTO substrate and exhibits an atomically smooth step-terrace surface, as shown in supplementary material Fig. S1. Figures 1(a) and 1(b) show temperature-dependent PFM phase and amplitude loops of the BTO/NbSTO heterostructure, in which typical hysteretic character with an 180° phase contrast is observed from 300 to 513 K. These suggest that ferroelectric nature with switchable polarization can persist up to 513 K in the 4 u.c.-thick BTO barrier that has improved c/a ratio of ~1.08 due to lattice mismatch.[16] Similar phenomena have

a)Author to whom correspondence should be addressed: zwen@qdu.edu.cn

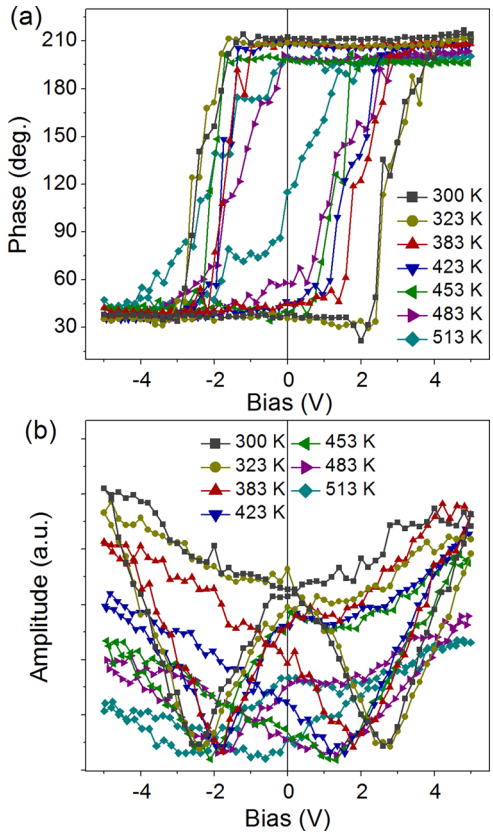

FIG. 1. PFM phase (a) and (b) amplitude hysteresis loops of the BTO/NbSTO heterostructure with increasing temperature from 300 to 513 K.

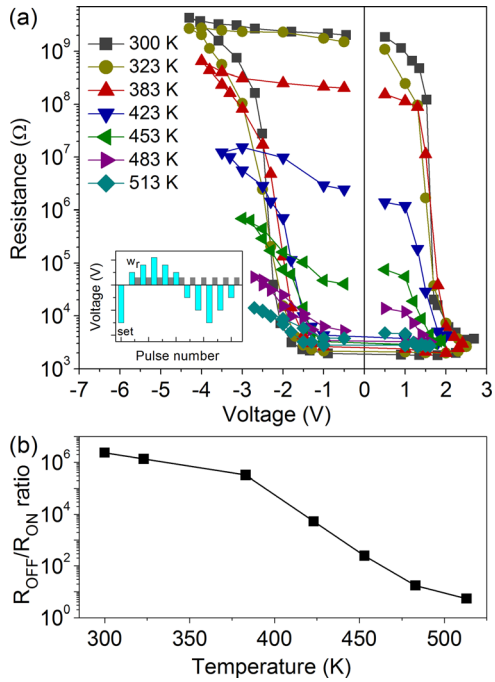

FIG. 2. (a) Temperature-dependent *R-V* hysteresis loops of the Pt/BTO/NbSTO FTJ measured by the pulse train shown schematically in the inset, which is composed of a set pulse (set) at −4.0 V, write pulses (w) following a triangular profile, and read pulses (r) at 0.3 V. Both the write and the read pulses are 1.0 ms in width. (b) The R_{OFF}/R_{ON} ratio as a function of temperature.

also been observed in compressively strained BTO thin films grown on $DyScO_3$ and $GdScO_3$ substrates, which exhibit ferroelectric-paraelectric transition at 813 and 673 K, respectively.[30] In addition, the PFM amplitude in Fig. 1(b) decreases with increasing temperature, indicating the decrease of polarization in the BTO barrier. According to the theoretical calculation by Pertsev *et al.*, this reduction can be ascribed to the temperature-dependent coefficients of the second-order polarization terms in the thermodynamic potential of epitaxial ferroelectric films.[31,32] The calculated ferroelectric double-well potentials of fully strained BTO film on $SrTiO_3$ substrate are shown in supplementary material Fig. S2 for clarity, in which the polarization decreases with increasing temperature, in agreement with that observed in Fig. 1(b).

As shown in Fig. 2(a), the Pt/BTO/NbSTO FTJ exhibits hysteretic resistance-voltage (*R-V*) loops from 300 to 513 K. As reported previously, the transport of 4 u.c.-thick Pt/BTO/NbSTO device is predominantly controlled by interfacial Schottky barrier.[29] By applying negative voltage, the BTO polarization is switched pointing to the Pt electrode, and the Schottky barrier is enhanced with the increased depletion region on NbSTO surface. The transport is suppressed, and the device is switched to the high resistance OFF state. When positive pulses are applied on the Pt electrode, the BTO polarization is switched, and the Schottky barrier is annihilated by electron accumulation on the NbSTO surface. The device is thus switched to the low resistance ON state. Figure 2(b) shows the R_{OFF}/R_{ON} ratio as a function of temperature, which is $\sim 2 \times 10^6$ at 300 K and decreases slightly to $\sim 3 \times 10^5$ at 383 K. With the further increase in temperature, the TER ratio exhibits an obvious decrease, which drops to ~5 at 513 K. The degradation of TER performance can be ascribed to the decrease of BTO polarization, as indicated by the temperature-dependent PFM amplitude loops shown in Fig. 1(b).

Temperature-dependent current-voltage (*I-V*) curves of the Pt/BTO/NbSTO FTJ for the OFF and the ON states are shown in Figs. 3(a) and 3(b), respectively. In the OFF state, the transport is predominantly governed by the interfacial Schottky barrier,[29] and a rectifying feature is observed from 300 to 513 K [Fig. 3(a)]. The OFF state current increases monotonically with increasing temperature. However, temperature-dependent transport is complicated in the ON state. As shown in Fig. 3(b), the *I-V* curves are symmetrical at 300, 323, and 383 K and develop progressively to a rectifying conduction as temperature further increases, associated with an obvious current decrease observed at the reverse bias. The *I-V* curves in linear style are shown in supplementary material Fig. S3 for clarity. For the forward bias, the current read at 0.1 V is plotted in the inset, which increases slightly from 300 to 383 K but drops sharply at higher temperature.

The transport mechanism is further analyzed by fitting the *I-V* curves to different conduction models. With a Schottky barrier, the OFF state transport may be governed by either the thermionic emission or the electron tunneling.[33,34] If the thermionic emission is dominant, the current density (J_F) at forward bias can be described by[35–37]

$$J_F = A^* T^2 \exp(-\phi_B / k_B T) \exp(qV / nk_B T), \quad (1)$$

where A^* is the effective Richardson constant,[36] T the absolute temperature, ϕ_B the Schottky barrier height, k_B the Boltzmann constant, q the electron charge, and n the ideality factor. The slope extracted from the fitting of lnJ_F-V by Eq. (1) is plotted in Fig. 4(c). As shown, the linear increase of

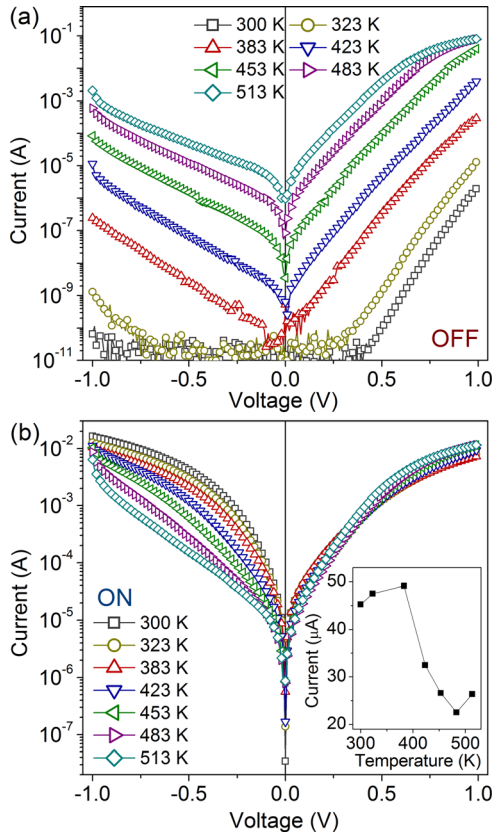

FIG. 3. Temperature-dependent semi-log *I-V* curves of the Pt/BTO/NbSTO FTJ for (a) the OFF and (b) the ON state, respectively. The inset in (b) is the ON state current, read at 0.1 V, as a function of temperature.

the slope with $1/T$ indicates the dominance of thermionic emission in the OFF state transport.[33,34] Therefore, ϕ_B can be deduced from the intercept in Fig. 4(a), which decreases from 0.96 to 0.76 eV with increasing temperature from 300 to 513 K, as shown in the inset in Fig. 4(c). As a result, the OFF state current exhibits a monotonic increase. However, the J_F of a metal/semiconductor junction also increases with increasing temperature because of the increase in thermal emission, even though there is no change in the potential barrier itself. We thus assume that the ϕ_B (=0.96 eV) does not change with temperature and calculate temperature-dependent J_F according to Eq. (1). As shown in supplementary material Fig. S4, the deviation of measured J_F from the calculated value becomes pronounced with increasing temperature, and the actual J_F is finally more than two orders of magnitude larger than the calculated value at 513 K, demonstrating the reduction of Schottky barrier at high temperature.

To clarify the function of BTO polarization in the OFF state, we measure temperature-dependent *I-V* curves of a Pt/NbSTO Schottky junction. The lnJ_F-V slopes extracted from the linear fits (Fig. S5, supplementary material) are plotted in Fig. 4(c) for comparison. It is obvious that the slope of Pt/NbSTO is almost constant with $1/T$. Similar phenomena have also been observed in NbSTO-based Schottky and *p-n* junctions and ascribed to the dominance of tunneling in the transport,[33,34,38] i.e., the field emission near the Fermi level (E_F) through the interfacial barrier, which is described by $J_F \propto \exp(qV/E_{00})$, where $E_{00} = \frac{q\hbar}{2}\sqrt{\frac{N}{m_n^*\varepsilon_0\varepsilon_d}}$ (ε_0 is the vacuum permittivity, ε_d the relative dielectric constant of NbSTO, m_n^* the effective electron mass, $\hbar$ the reduced Planck constant, and N the doping concentration).[35] Therefore, without the ferroelectric BTO layer, the Pt/NbSTO junction exhibits a different transport behavior since there is no polarization-enhancement on the depletion region and hence the Schottky barrier.

Temperature-dependent capacitance is measured to estimate the change of depletion region width (W_d) on the NbSTO surface. As shown in Fig. 4(d), the capacitance of the Pt/NbSTO is almost independent upon temperature, which is 80.8 pF at 300 K and increases slightly to 81.6 pF at 423 K. The measured capacitance becomes unreasonably large at higher temperature because a resonance peak appears in the capacitance-frequency curve near 3 MHz. In contrast, the OFF state capacitance of the Pt/BTO/NbSTO FTJ increases significantly with increasing temperature. In this device, the depletion region is in series with the BTO barrier, and the measured

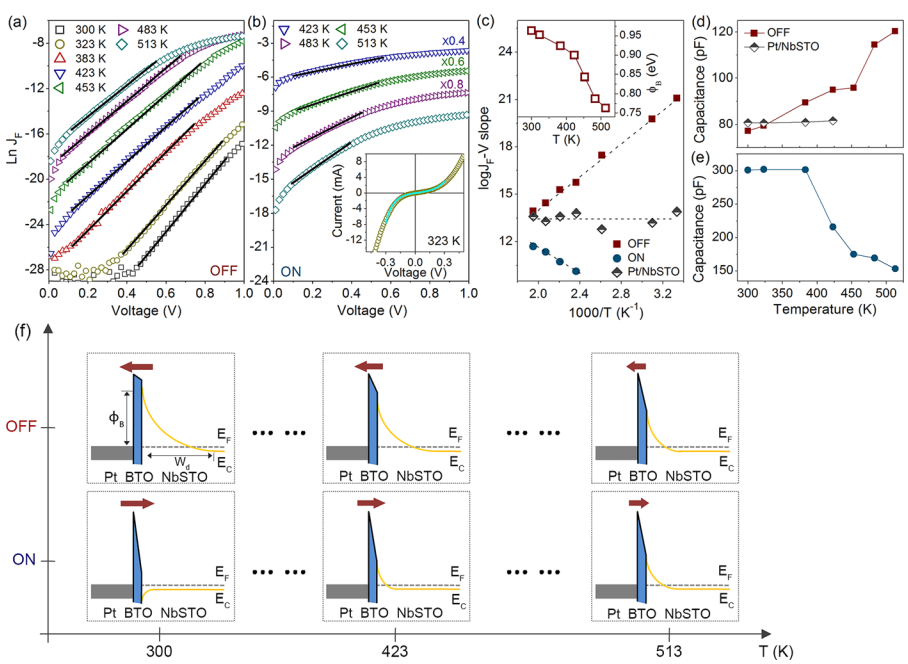

FIG. 4. LnJ_F-V plots of the Pt/BTO/NbSTO FTJ for (a) the OFF and (b) the ON state, in which the black solid lines are linear fits. For clarity, the ON state lnJ_F-V plots are rescaled. The inset in (b) is the ON state *I-V* curve at 323 K, in which the cyan solid line is fit to the direct tunneling model. (c) $LogJ_F$-V slope versus $1000/T$ plots for the OFF and the ON state of the Pt/BTO/NbSTO FTJ, as well as for the Pt/NbSTO junction, where the dashed lines are a guide to the eye. The inset in (c) is the OFF state ϕ_B as a function of temperature. (d) The OFF state capacitance of the Pt/BTO/NbSTO as a function of temperature, where the temperature-dependent capacitance of the Pt/NbSTO is also shown for comparison. (e) The ON state capacitance of the Pt/BTO/NbSTO as a function of temperature. (f) Schematic description of the evolution of the Schottky barrier profile with increasing temperature, where the red arrow denotes the BTO polarization.

capacitance (C_0) can be expressed as $1/C_0 = 1/C_{BTO} + 1/C_d$, in which C_{BTO} is the capacitance of the BTO barrier, which can be obtained from the ON state capacitance since the depletion region is annihilated, as discussed below, and $C_d = \varepsilon_0\varepsilon_d A/W_d$ is the capacitance of the depletion region, where A is the junction area.[35] Therefore, the increased capacitance observed in Fig. 4(d) indicates the decrease of W_d. With ϕ_B and W_d, temperature-dependent Schottky barrier profile can be revealed. As depicted in Fig. 4(f), the Schottky barrier is reduced in both the height and the width with increasing temperature, which can be explained in terms of the decrease of BTO polarization. In the OFF state, the negative ferroelectric bound charges at the BTO/NbSTO interface are compensated by the ionized donors in the depletion region. As the polarization decreases, the W_d decreases and hence the Schottky barrier is reduced correspondingly.

When BTO polarization is switched pointing to the NbSTO, the Pt/BTO/NbSTO FTJ is set to the ON state. From 300 to 383 K, the I-V curves shown in Fig. 3(b) are nonlinear with applied voltage. The direct tunneling model, based on a trapezoidal-shape potential barrier, is adopted to describe the transport character, which is given by[4,39]

$$J = C\frac{\exp\left\{\alpha(V)\left[\left(\phi_2 - \frac{eV}{2}\right)^{3/2} - \left(\phi_1 + \frac{eV}{2}\right)^{3/2}\right]\right\}}{\alpha^2(V)\left[\left(\phi_2 - \frac{eV}{2}\right)^{1/2} - \left(\phi_1 + \frac{eV}{2}\right)^{1/2}\right]^2} \times \sinh\left\{\frac{3}{2}\alpha(V)\left[\left(\phi_2 - \frac{eV}{2}\right)^{1/2} - \left(\phi_1 + \frac{eV}{2}\right)^{1/2}\right]\frac{eV}{2}\right\}, \quad (2)$$

where $C = -(4em_n^*)/(9\pi^2\hbar^3)$ and $\alpha(V) = [4d(2m_n^*)^{1/2}]/[3\hbar(\phi_1 + eV - \phi_2)]$, ϕ_1 (ϕ_2) is the barrier height at the Pt/BTO (BTO/NbSTO) interface and d is the BTO barrier width. As shown in the inset in Fig. 4(b), the I-V curve at small bias range can be fitted using Eq. (2) with reasonable parameters of $\phi_1 = 1.6$ eV, $\phi_2 = 0.2$ eV, and $d = 1.6$ nm, respectively. The validity of the direct tunneling model suggests that the ON state transport is governed by the trapezoidal BTO barrier and the NbSTO surface is accumulated by electrons. It is worth noting that thermally activated conduction, such as phonon-assisted indirect tunneling via the localized states inside the BTO barrier, may also exist in parallel with the direct tunneling, especially for the currents measured above room temperature.[12,40,41] Therefore, the barrier height extracted from Eq. (2) might be underestimated. With the further increase in temperature from 423 to 513 K, the forward bias current exhibits an exponential increase with voltage in the range of 0.1–0.5 V [Fig. 4(b)], and the I-V curve becomes more and more asymmetrical [Fig. 3(b)], suggesting the emergence of the Schottky barrier. The evolution of the ON state barrier is also corroborated by the temperature-dependent capacitance shown in Fig. 4(e). The ON state capacitance is almost constant from 300 to 383 K since the NbSTO surface is accumulated by a high density of electrons to compensate the positive ferroelectric charges, and the depletion region, resulting from the difference in E_F between the Pt and the NbSTO, is completely annihilated. The measured capacitances are only from the BTO barrier, i.e., the C_{BTO}. As temperature increases, the density of aggregated electrons decreases with decreasing polarization. The NbSTO surface is no longer accumulated at 423 K, and the Schottky barrier reappears in the uncompensated depletion region. As a result, the ON state capacitance starts to drop because of the increase in overall barrier width. The current is also reduced [Fig. 3(b)]. The monotonic decrease of the capacitance suggests the increase of W_d and the enhancement of the Schottky barrier with increasing temperature from 423 to 513 K. The high-temperature I-V curves are further analyzed by linear fitting, and the extracted lnJ_F-V slopes are plotted versus $1/T$, as shown in Figs. 4(b) and 4(c). The ON state slope increases with increasing temperature, which are different from that observed in the OFF state and in the Pt/NbSTO junction. Obviously, the ON state W_d cannot be larger than that of the Pt/NbSTO,[29] and the field emission may also be dominant. In this case, the temperature-dependent slope behavior observed in the ON state may be ascribed to the development of the Schottky barrier. It has been reported that dielectric constant of NbSTO increases with decreasing electron density.[42] In the Pt/BTO/NbSTO with decreasing polarization, the ε_d of the NbSTO surface might increase as the widening of the depletion region, resulting in the decrease in E_{00} with increasing temperature.

Overall, as shown in Fig. 4(f), the polarization-modulation on junction barrier between the OFF and the ON state becomes small with increasing temperature since the Schottky barrier is reduced in the OFF state but it reappears and enhances in the ON state, which results in the gradual reduction of R_{OFF}/R_{ON} ratio. High-temperature retention properties of the Pt/BTO/NbSTO FTJ are shown in Fig. 5(a). The retention time for a R_{OFF}/R_{ON} ratio of ~10 at 423, 453, and 483 K is plotted in Fig. 5(b) as a function of $1/k_BT$ following an Arrhenius-type

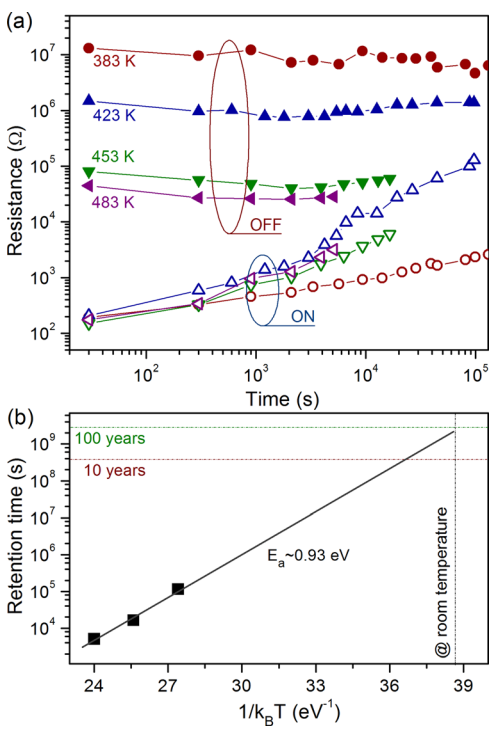

FIG. 5. (a) Retention properties of the Pt/BTO/NbSTO FTJ at high temperature and (b) retention time at 423, 453, and 483 K versus $1/k_BT$.

relation $\tau = \tau_0 \exp(E_a/k_B T)$, where τ is the retention time, τ_0 a constant, and E_a the activation energy. The E_a extracted from the linear fitting is ~0.93 eV, which is comparable to that of commercial FeRAMs.[22,23] In addition, the room-temperature retention time of the Pt/BTO/NbSTO device is estimated by the extrapolation of retention time with temperature, which can be as long as ~70 years.

In summary, high-temperature TER properties of the Pt/BTO/NbSTO FTJ have been demonstrated. A giant R_{OFF}/R_{ON} ratio of $\sim 3 \times 10^5$ can be maintained up to 383 K even though the TER performance degrades with increasing temperature. The reduction of TER ratio can be ascribed to the decrease of BTO polarization, which results in the reduction of ferroelectric-modulation on junction barrier between the OFF and the ON state. By fitting the retention time at elevated temperature, the E_a for a R_{OFF}/R_{ON} ratio ~10 can be deduced to be ~0.93 eV and the room-temperature retention time can be estimated to be ~70 years. These results suggest excellent endurance of the Pt/BTO/NbSTO FTJ devices above room temperature. In addition, the temperature-dependent transport behaviors and the associated evolution of the Schottky barrier observed in this study provide experimental evidence for ferroelectric-driven resistive memory in the MFS FTJs, as the TER effect decreases and tends to vanish with decreasing polarization. On the other hand, the present work also facilitates the design of multifunctional metal/semiconductor devices, such as the recent progress in $SrRuO_3$/n-type BTO interface, in which the polarization reversal not only gives rise to an Ohmic to Schottky transition but also controls spin injection from the ferromagnetic electrode.[43,44]

See supplementary material for the surface topography of BTO/NSTO heterostructure, the thermodynamic calculation for fully strained BTO film, the evolution of ON state transport with increasing temperature, the comparison of the OFF state J_F between the measured and calculated values, and the *I-V* curves of the Pt/NbSTO junction.

This work was jointly sponsored by National Natural Science Foundation of China (Grant Nos. 11574169, 51472131, and 11504193), the Hong Kong Scholars Program (XJ2015024), and an innovation project of Qingdao (17-1-1-71-jch).

[1]E. Y. Tsymbal and H. Kohlstedt, Science **313**, 181 (2006).
[2]V. Garcia and M. Bibes, Nat. Commun. **5**, 4289 (2014).
[3]M. Ye. Zhuravlev, R. F. Sabirianov, S. S. Jaswal, and E. Y. Tsymbal, Phys. Rev. Lett. **94**, 246802 (2005).
[4]D. Pantel and M. Alexe, Phys. Rev. B **82**, 134105 (2010).
[5]J. P. Velev, J. D. Burton, M. Ye. Zhuravlev, and E. Y. Tsymbal, npj Comput. Mater. **2**, 16009 (2016).
[6]H. Kohlstedt, N. A. Pertsev, J. R. Contreras, and R. Waser, Phys. Rev. B **72**, 125341 (2005).
[7]M. Gajek, M. Bibes, S. Fusil, K. Bouzehouane, J. Fontcuberta, A. Barthélémy, and A. Fert, Nat. Mater. **6**, 296 (2007).
[8]V. Garcia, S. Fusil, K. Bouzehouane, S. Enouz-Vedrenne, N. D. Mathur, A. Barthélémy, and M. Bibes, Nature **460**, 81 (2009).
[9]D. Pantel, S. Goetze, D. Hesse, and M. Alexe, Nat. Mater. **11**, 289 (2012).
[10]A. Chanthbouala, A. Crassous, V. Garcia, K. Bouzehouane, S. Fusil, X. Moya, J. Allibe, B. Dlubak, J. Grollier, S. Xavier, C. Deranlot, A. Moshar, R. Proksch, N. D. Mathur, M. Bibes, and A. Barthélémy, Nat. Nanotechnol. **7**, 101 (2012).
[11]F. Y. Bruno, S. Boyn, S. Fusil, S. Girod, C. Carrétéro, M. Marinova, A. Gloter, S. Xavier, C. Deranlot, M. Bibes, A. Barthélémy, and V. Garcia, Adv. Electron. Mater. **2**, 1500245 (2016).
[12]Y. W. Yin, J. D. Burton, Y.-M. Kim, A. Y. Borisevich, S. J. Pennycook, S. M. Yang, T. W. Noh, A. Gruverman, X. G. Li, E. Y. Tsymbal, and Q. Li, Nat. Mater. **12**, 397 (2013).
[13]H. Lu, A. Lipatov, S. Ryu, D. J. Kim, H. Lee, M. Ye. Zhuravlev, C.-B. Eom, E. Y. Tsymbal, A. Sinitskii, and A. Gruverman, Nat. Commun. **5**, 5518 (2014).
[14]L. F. Wang, M. R. Cho, Y. J. Shin, J. R. Kim, S. Das, J.-G. Yoon, J.-S. Chung, and T. W. Noh, Nano Lett. **16**, 3911 (2016).
[15]M. Ye. Zhuravlev, Y. Wang, S. Maekawa, and E. Y. Tsymbal, Appl. Phys. Lett. **95**, 052902 (2009).
[16]Z. Wen, C. Li, D. Wu, A. Li, and N. Ming, Nat. Mater. **12**, 617 (2013).
[17]W. J. Hu, Z. Wang, W. Yu, and T. Wu, Nat. Commun. **7**, 10808 (2016).
[18]D. S. Jeong, R. Thomas, R. S. Katiyar, J. F. Scott, H. Kohlstedt, A. Petraru, and C. S. Hwang, Rep. Prog. Phys. **75**, 076502 (2012).
[19]C. S. Hwang, Adv. Electron. Mater. **1**, 1400056 (2015).
[20]K. Lee, M. Kang, Y. Hwang, and H. Shin, IEEE Trans. Electron Devices **63**, 659 (2016).
[21]K. Lee, M. Kang, S. Seo, D. Kang, S. Kim, D. H. Li, and H. Shin, IEEE Trans. Electron Devices **60**, 1099 (2013).
[22]T. D. Hadnagy and D. J. Sheldon, Integr. Ferroelectr. **4**, 217 (1994).
[23]F. Chu, G. Fox, and T. Davenport, Integr. Ferroelectr. **36**, 43 (2001).
[24]M. A. Khan, U. S. Bhansali, M. N. Almadhoun, I. N. Odeh, D. Cha, and H. N. Alshareef, Adv. Funct. Mater. **24**, 1372 (2014).
[25]M. Q. Cai, Y. Du, and B. Y. Huang, Appl. Phys. Lett. **98**, 102907 (2011).
[26]J. Woo, S. Hong, D. K. Min, H. Shin, and K. No, Appl. Phys. Lett. **80**, 4000 (2002).
[27]J. H. Park, C. W. Byun, K. H. Seok, H. Y. Kim, H. J. Chae, S. K. Lee, S. W. Son, D. C. Ahn, and S. K. Joo, J. Appl. Phys. **116**, 124512 (2014).
[28]T. Bang, B. H. Lee, C. K. Kim, D. C. Ahn, S. B. Jeon, M. H. Kang, J. S. Oh, and Y. K. Choi, IEEE Electron Device Lett. **38**, 40 (2017).
[29]Z. Xi, J. Ruan, C. Li, C. Zheng, Z. Wen, J. Dai, A. Li, and D. Wu, Nat. Commun. **8**, 15217 (2017).
[30]K. J. Choi, M. Biegalski, Y. L. Li, A. Sharan, J. Schubert, R. Uecker, P. Reiche, Y. B. Chen, X. Q. Pan, V. Gopalan, L. Q. Chen, D. G. Schlom, and C.-B. Eom, Science **306**, 1005 (2004).
[31]N. A. Pertsev, A. G. Zembilgotov, and A. K. Tagantsev, Phys. Rev. Lett. **80**, 1988 (1998).
[32]N. A. Pertsev, A. G. Zembilgotov, S. Hoffmann, R. Waser, and A. K. Tagantsev, J. Appl. Phys. **85**, 1698 (1999).
[33]D. S. Shang, J. R. Sun, L. Shi, J. Wang, Z. H. Wang, and B. G. Shen, Appl. Phys. Lett. **94**, 052105 (2009).
[34]E. Lee, M. Gwon, D. W. Kim, and H. Kim, Appl. Phys. Lett. **98**, 132905 (2011).
[35]S. M. Sze and K. K. Ng, *Physics of Semiconductor Devices*, 3rd ed. (John Wiley & Sons, Inc., Hoboken, New Jersey, 2007) p. 134.
[36]S. Suzuki, T. Yamamoto, H. Suzuki, K. Kawaguchi, K. Takahashi, and Y. Yoshisato, J. Appl. Phys. **81**, 6830 (1997).
[37]E. Mikheev, B. D. Hoskins, D. B. Strukov, and S. Stemmer, Nat. Commun. **5**, 3990 (2014).
[38]Y. W. Xie, J. R. Sun, D. J. Wang, S. Liang, W. M. Lü, and B. G. Shen, Appl. Phys. Lett. **90**, 192903 (2007).
[39]A. Gruverman, D. Wu, H. Lu, Y. Wang, H. W. Jang, C. M. Folkman, M. Ye. Zhuravlev, D. Folker, M. Rzchowski, C.-B. Eom, and E. Y. Tsymbal, Nano Lett. **9**, 3539 (2009).
[40]Y. Xu, A. Matsuda, and M. R. Beasley, Phys. Rev. B **42**, 1492 (1990).
[41]Z. Wen, L. You, J. Wang, A. Li, and D. Wu, Appl. Phys. Lett. **103**, 132913 (2013).
[42]T. Fujii, M. Kawasaki, A. Sawa, Y. Kawazoe, H. Akoh, and Y. Tokura, Phys. Rev. B **75**, 165101 (2007).
[43]X. Liu, Y. Wang, J. D. Burton, and E. Y. Tsymbal, Phys. Rev. B **88**, 165139 (2013).
[44]X. Liu, J. D. Burton, M. Ye. Zhuravlev, and E. Y. Tsymbal, Phys. Rev. Lett. **114**, 046601 (2015).